Proceedings of the IMProVe 2011
International conference on Innovative Methods in Product Design
June 15th – 17th, 2011, Venice, Italy

Geometric processing of GeoEye-1 satellite imagery for coastal mapping applications

Manuel Ángel Aguilar [(a)], Fernando J. Aguilar [(a)], Antonio Fernández [(b)], Ismael Fernández [(a)], María del Mar Saldaña [(a)], Andrés M. García Lorca [(c)]; João G. Negreiros [(d)]; Alfonso Viciana [(e)]; Elena González [(b)]

[(a)] Dept. of Agricultural Engineering, University of Almería,
[(b)] Dept. of Engineering Design, Universidad de Vigo, Escuela Técnica Superior de Ingeniería Industrial,
[(c)] Dept. Geography and History of the Art, University of Almería,
[(d)] ISEGI, Universidade Nova de Lisboa,
[(e)] Dept. Geographical Regional Analysis, UNED, Universidad Nacional de Educación a Distancia

Article Information

Keywords:
Satellite imagery,
Orthorectification,
Classification,
Accuracy,
DEM.

Corresponding author:
Manuel Ángel Aguilar
Tel.: 950015950
Fax.: 950015491
e-mail: maguilar@ual.es
Address: University of Almería, La Cañada de San Urbano s/n, 04120 Almería, Spain

Abstract

In 2008 and with the cooperation of the U.S. Department of Defence, it was launched a new commercial very high resolution (VHR) satellite named GeoEye-1 (GeoEye, Inc.) which, nowadays, is the commercial satellite with the best geometric resolution, so much in panchromatic (0.41m) as in multispectral (1.65m). More recently, on January 4, 2010, DigitalGlobe have begun to commercialize imagery of the last of the VHR satellites launched: WorldView-2. Its most relevant technical innovation includes the radiometric accuracy improvement, since the number of bands that compose its multispectral image has increased to 8, instead of the 4 classic bands (R, G, B, NIR) of the previous VHR satellites.
These new VHR satellites offer important improvements closely related to spatial and spectral resolution. Therefore, an improvement is awaited in: (i) the geometric accuracies obtained in orthoimages and digital elevation models (DEMs) generated from scenes of GeoEye-1 and WorldView-2, as well as, (ii) an increase in the accuracy of the objects classification (urbanizations, buildings, highways, impervious zones, crops). These possible improvements will have to be contrasted with real tests carried out in field conditions, studying the ideal performance procedures in the seeking of accurate geo-referenced information.
In this work the geometric accuracy of a single panchromatic image of GeoEye-1 with an off-nadir angle higher than 20 degrees was researched. Rational Polynomial Coefficients refined by a zero order polynomial adjustment (RPC0) was the sensor model that generated the best results. Using a DEM with a vertical accuracy of about 1.34 m, accurate orthoimages (planimetric root mean square error of 0.87 m) can be obtained from GeoEye-1 imagery.

1 Introduction

John Croft [1] began his paper titled “Prodigious mapping capabilities, spatial resolution and geo-location ability of the GeoEye’s next-generation imaging satellite” remembering as, in 1900, in the magazine Ladies Home Journal, an article making predictions for the next century said, “Flying machines will carry powerful telescopes that beam back to Earth photographs as distinct and large as if taken from across the street”. With the launch of the first very high resolution (VHR) satellites, IKONOS in September 1999, with 1 m as the nominal ground sample distance (GSD) in panchromatic, and QuickBird in October 2001, with 0.61m as the nominal GSD, that one-hundred-year-old prediction from Ladies Home Journal has come true, almost right on time.

Besides, many new VHR satellites, capable of capturing panchromatic imagery of the land surface with GSD of 1 m and even lower, such as EROS B1, Resurs DK-1, KOMPSAT-2, IRS Cartosat 2, WorldView-1, have been launched during 2006 and 2007, and they are offering to their customers very high resolution imagery of the Earth, with a revisit time very shortly. The rapid increase of commercial VHR satellites in the next few years will result in improvements in resolution, availability and cost. Thus, conventional aerial photogrammetric mapping at large scales began to have serious competitors [2], [3], [4], [5] and [6]. In fact, IKONOS and QuickBird offers the possibility of fast and accurate generation of orthoimages, improving the generated from conventional photogrammetric flights, like for example, the B&W Andalusia’s orthoimage of 2002 [8].

Besides, this type of satellite images have been used for numerous applications in: (i) building detection [9], [10], [11], [12], [13], [14] and [15], (ii) road extraction [16] and [17], (iii) vegetation studies [18] and [19], (iv) greenhouses delineation [20] and [21], (v) location of

damages caused by natural disasters [22], and assessing canopy mortality [23].

In 2008 a new commercial VHR satellite named GeoEye-1 (GeoEye, Inc.) was launched. Nowadays, it is the commercial satellite with the highest geometric resolution, in panchromatic (0.41 m) and in multispectral (1.65 m). The first results obtained with scenes of GeoEye-1 are superior enough to that they had been obtained till now using scenes of other commercial satellites of very high resolution such as IKONOS or QuickBird. Fraser and Ravanbakhsh [24] have obtained vertical and horizontal accuracies of 0.25 m and 0.10 m respectively using a stereo-pair of GeoEye-1. John Croft [1] qualified as prodigious the capacities of GeoEye-1 for the generation of maps.

More recently, Digital Globe Inc. has launched their last VHR satellite, WorldView-2. Although it also presents a very high geometric resolution (0.46 m and 1.84 m as the nominal GSD in panchromatic and multispectral respectively), its most relevant technical innovation is the radiometric accuracy improvement, since the number of bands that compose its multispectral image has increased to 8, instead of the 4 classic bands (i.e., Red (R), Green (G), Blue (B) and Near Infrared (NIR)) of the previous VHR satellites. The images of this new VHR satellite have been started commercializing from January 4, 2010. Thus, there is not many published works about its applications. Nevertheless, according to a pilot study fulfilled by DigitalGlobe [25], substantial improvements can be obtained in the accuracy of the classification using all 8 bands of WorldView-2, opposite to the multispectral traditional RGB-NIR images from QuickBird, IKONOS or GeoEye-1. These improvements were quantified in a global improvement from 10 to 30 % in the classification of highways, vegetation or aquatic elements (reefs, barriers of sand). On the other hand, similar to WorldView-1, QuickBird, IKONOS or GeoEye-1 data, it is possible to achieve geometric accuracies in the orientation phase within 1 m as Root Mean Square Error (RMSE) using very few accurate Ground Control Points (GCPs) for WorldView-2 data.

This work is presented in the frame of two Research Projects recently funded by both, the Spanish Ministry for Science and Innovation (CTM2010-16573), and the Andalusia Regional Government (RNM-3575). These projects are focused in the monitoring and modelling of the evolution and vulnerability of coastal areas. In that Research Project multi-source (including VHR satellite imagery) and multi-temporal geospatial data (from 1956 to nowadays) are being integrated in a pilot area located at a coastal fringe of Almería, Spain.

The main objective of the Spanish Ministry's project is to study the actual accuracy and quality obtained, in operational conditions, in the geo-referenced information (orthoimages, digital elevation models (DEMs) and maps compiled from detected objects gathered by classification software) generated from imagery of the commercial VHR satellites more innovative and unexplored, i.e., GeoEye-1 and WorldView-2.

Compared with its predecessors, these new VHR satellites offer important improvements closely related to their spatial and spectral resolution. Therefore, a sensitive improvement may be expected in: (i) the geometric accuracies obtained in orthoimages and DEMs generated from scenes of GeoEye-1 and WorldView-2, as well as, (ii) an increase in the accuracy of the objects classification (urbanizations, buildings, highways, impervious areas, crops), owed to the higher number of bands that compose the multispectral image of WorldView-2. These potential improvements will have to be contrasted with real tests in fields conditions, studying the ideal and optimised methodologies for the generation of geo-referenced information as accuracy as possible.

The geo-referenced data generated from VHR satellite scenes present important capabilities headed-up to objects classification, especially in coastal zones (e.g., using of the Coastal Blue band from WorldView-2 for obtaining near shore bathymetry). Hence they will be used for the monitoring of the coastal fringe placed between Garrucha and Villaricos (Almería), where the construction of an artificial channel of the river Almanzora and the proliferation of urbanizations during the last 50 years have provoked serious natural disasters, e.g., the loss of about 200 m of cross-shore beach at Quitapellejos area (Palomares).

In this work, the first results obtained from the aforementioned research project coded as CTM2010-16573 are going to be presented. Concretely, the geometric accuracy capabilities of GeoEye-1 Panchromatic Geo image will be investigated. Also, the orthoimages generated from GeoEye-1 (September, 2010) and from a historical photogrammetric flight named as "American flight" (September, 1956) will be compared at the study site.

2 Study site

The study area comprises the heavily developed coastal fringe of Almería (Mediterranean Sea, Southern Spain), approximately 11 km long and 775 m wide. The working area is situated between the harbours of Garrucha and Villaricos (Fig. 1), and is centred on the WGS84 coordinates (easting and northing) of 605870 m and 4119869 m.

Fig. 1 Situation of the selected pilot zone. Vectorial details on the Orthoimage by Andalusia Government (1998-99) with a GSD of 1 m.

In the last half century this zone seems to have a terrible curse. First was the tragic incident resulting in the contamination of a 2 km^2 by radioactive plutonium occurred on January 17, 1966, when a B-52G bomber of the USAF Strategic Air Command carried four Mk28 type hydrogen bombs collided with a KC-135 tanker during mid-air refuelling at 9450 m over the Mediterranean Sea, near the small fishing village of Palomares, in the municipality of Cuevas del Almanzora, Almería, Spain. On the other hand, the proliferation of urbanization in this coastal fringe during the last 50 years has provoked significant changes in its landscape, and induced serious natural disasters.

3 Datasets

3.1 American flight (1956)

1956 photography was the first datasets used in this study. It was acquired using a "standard" metric camera format of 230 x 230 mm. From a historic perspective, this dataset is interesting since it was the first photogrammetric project to cover the majority of Spain. Undertaken by the U.S. Government, it is referred to in Spain as the "American flight". In most parts of Spain the historical record of metric aerial photography began with this flight. It is therefore regarded as a valuable national information source for photo-interpretation and land use evolution.

The original negatives were scanned using a photogrammetric scanner with a geometric resolution of 21 µm and a radiometric resolution of 8 bits, and stored in TIFF format giving a GSD of approximately 0.70 m. The digitized photographs were provided by the Network of Environmental Information of Andalusia (known as REDIAM).

The orthoimage of this flight was generated by us using ancillary data (GCPs and DEM) which are going to be explained later.

3.2 GeoEye-1 satellite image

In January 2011, we acquired an archive image of GeoEye-1 Geo (bundle Panchromatic and Multispectral). It was taken on 29 September 2010. The clip of the image was occupying approximately 50 km^2 and was centred on the study area. Other characteristics of the GeoEye-1 image are shown in Tab. 1. In this work we have only used the panchromatic image.

Product	GeoEye-1 Geo
Acquisition Date	29/09/10
Cloud Cover (%)	0
Scene Identifier	2010092911015041603031603264_004
Sun Angle Azimuth	159.29 degrees
Sun Angle Elevation	48.39 degrees
Sensor Elevation Angle	69.41 degrees
Sensor Azimuth Angle	221.92 degrees
Acquired Nominal GSD	0.46 m
Product Pixel Size	0.50 m

Tab. 1 Characteristics of the GeoEye-1 Geo image acquired at the study site.

GeoEye-1 Geo is the GeoEye's commercial imagery format that presents the least level of corrections, both radiometric and geometric. Geo images include the camera geometry obtained at the time of the image collection. With the Geo imagery, users can produce their own highly accurate orthorectified products by utilizing commercial off the shelf software, DEMs, and GCPs.

3.3 Ground Control Points

The measurement of ground points (Ground Control Points, GCPs and Indendent Check Points, ICPs) was done using Differential Global Positioning System (DGPS) receivers in real-time kinematic (RTK) mode. The goal was to obtain a reliable measurement of ground points with accuracy better than a 0.10 m. As a final result of the methodology described the UTM ETRS89 coordinates were obtained as well as the orthometric elevations on 121 ground points. The selection of the GCPs and ICPs used in this study was based on well-defined and homogeneously distributed points over the study area (Fig. 2).

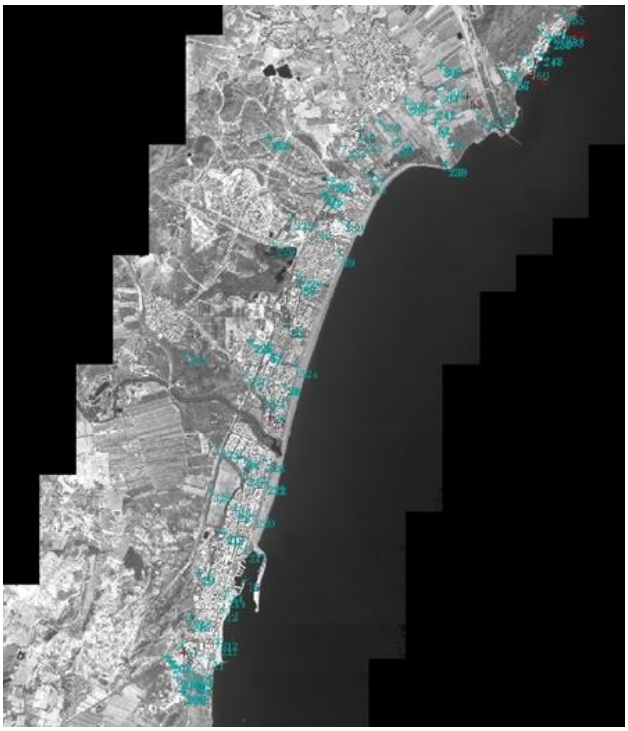

Fig. 2 Distribution of 121 ground points (GCPs and ICPs) overlaid on the GeoEye-1 Geo panchromatic image.

3.4 Digital Elevation Model

For the generation of panchromatic orthoimages from both GeoEye-1 Geo and American Flight, a DEM with a grid spacing of 10 m was used. This DEM was obtained by the Andalusia Government from a panchromatic photogrammetric flight at an approximate scale of 1:20000 realized during 2001-2002 (Fig. 3). The Andalusia DEM was published in 2005 [26].

This original DEM was transformed from UTM European Datum 1950 and orthometric heights to the new Spanish official geodetic system called the European Terrestrial Reference System (ETRS89) above GRS80 ellipsoid using the minimum curvature method developed by the Spanish Geographical National Institute (IGN). The corresponding DEM accuracy was estimated upon 62 DGPS check points located at open terrain, yielding a vertical RMSE value around 1.34 m [27].

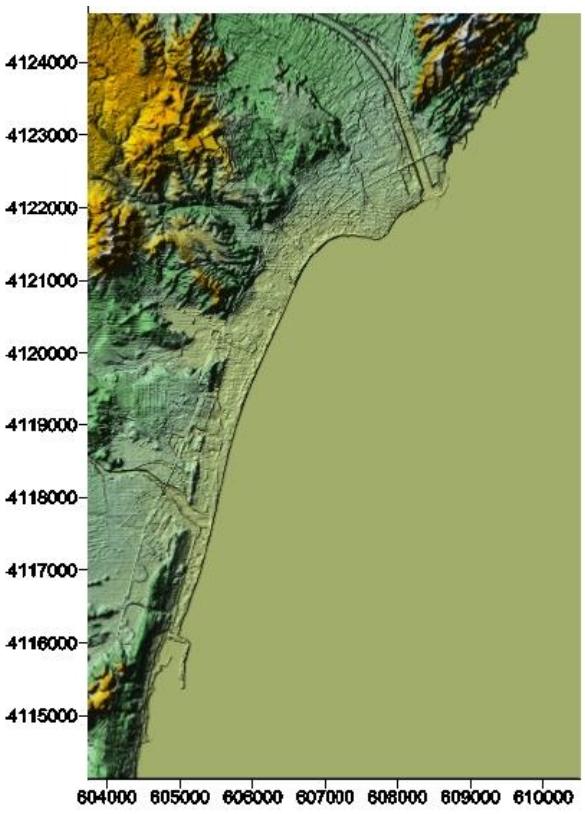

Fig. 3 DEM derived by Andalusia Government over the study area.

4 Sensor models used

In satellite imagery, a sensor model or geometric correction model relates object point positions (*X*, *Y*, *Z*) to their corresponding 2D image positions (*x*, *y*).

Several sensor models can be used to correct satellite imagery: 2D polynomial functions, 3D polynomial functions, affine model, 3D rational functions and 3D physical models, e.g., [28], [29] and [30]. PCI Geomatica OrthoEngine software v. 10.3.2, developed by PCI Geomatics was used for the four sensor models tested in this work:

1.- Third order 3D rational functions with vendor's rational polynomial coefficients (RPCs) data and refined by a zero order polynomial adjustment (RPC0).

The general form of 3D rational functions is:

$$x = \frac{P_1(X,Y,Z)}{P_2(X,Y,Z)}; y = \frac{P_3(X,Y,Z)}{P_4(X,Y,Z)} \quad (1)$$

Where *x* and *y* are the row and column in the image respectively, *X*, *Y* and *Z* are the coordinates of points in object space, and, *Pi* (*i*=1, 2, 3, and 4) are polynomial functions.

With the physical sensor model available for commercial satellite data vendors, rational polynomial coefficients (RPCs) can be solved using an object grid with its nodes coordinates determined by means of the physical sensor model [28]. Third order RPCs for the forward form are usually distributed by image vendor in VHR sensors, such as IKONOS, QuickBird or GeoEye-1.

This method can be applied without GCPs (this is why it also is known as terrain-independent), although the accuracy obtained is not very good. A very interesting aspect of this method is that users can update or improve the accuracy of the rational function model, refining the image vendor coefficients using a few GCPs. In VHR satellite imagery, the RPCs may be refined directly or indirectly [31]. The OrthoEngine RPC indirect method is based on the block adjustment method developed by Grodecki and Dial [32] for image space:

$$\Delta x = x' - x = a_0 + a_1 \cdot x + a_2 \cdot y$$
$$\Delta y = y' - y = b_0 + b_1 \cdot x + b_2 \cdot y \quad (2)$$

where a_0, a_1, a_2, b_0, b_1 and b_2 are the adjustment parameters of an image, Δx and Δy express the discrepancies between the line measured and the sample coordinates for the new GCPs in the image space (x', y') and the RCPs projected coordinates for the same GCPs (x, y).

For the zero order transformation, only a simple shift (a_0 and b_0) are computed. Because of it, only one GCP is necessary to calculate this indirect method. For IKONOS images, the zero order polynomial adjustment is adequate for most cases, while for QuickBird images a first order polynomial adjustment is required to achieve the best results [33].

2.- Third order 3D rational functions with vendor's RPCs data and refined by a first order polynomial adjustment (RPC1). In this case 6 coefficients of the equation 2 have to be computed. Therefore it is necessary to know at least three GCPs.

3.- Third order 3D rational functions with vendor's RPCs data and refined by a second order polynomial adjustment (RPC2). In this case 12 coefficients have to be computed (eq. 3). Therefore it is necessary to know at least six GCPs.

$$\Delta x = x' - x = a_0 + a_1 x + a_2 y + a_3 xy + a_4 x^2 + a_5 y^2$$
$$\Delta y = y' - y = b_0 + b_1 x + b_2 y + b_3 xy + b_4 x^2 + b_5 y^2 \quad (3)$$

4.- A 3D physical model developed by Dr. Toutin at the Canada Centre for Remote Sensing [34] is also tested in this work (CCRS) for the GeoEye-1 imagery. This physical model was initially developed for medium-resolution sensors in the visible and infra-red as well as in the microwave. Even though the detailed sensor information for GeoEye-1 has not been released by the vendor, a valid solution for CCRS can be obtained using a limited number of GCPs (around six) and basic information from the image metafiles.

5 Methodology

The error of the orthoimage can be expressed as the sum of the error in the sensor orientation phase plus the error due to the DEM (equation 4).

$$\sigma_{ortho}^2 = \sigma_o^2 + \sigma_{DEM}^2 \quad (4)$$

Where σ_{ortho} is the final two-dimensional error of the orthoimage, σ_o is the bundle adjustment error or sensor orientation error, and σ_{DEM} is the 2D orthoimage error propagated from the original DEM error. All the terms are expressed as standard deviations.

Equation 4 is based on the general error-propagation theory, assuming that the sources of error are independent or uncorrelated and, at the same time, these errors are randomly distributed. Notice that equation 4 can be expressed in terms of RMSE when the mean error tends to be zero (unbiased residuals).

In this work we have fundamentally studied the errors occurred at both the orientation or bundle adjustment phase and the final orthoimage. In all the cases studies in this work, 9 GCPs well-distributed and defined were used for computing the different sensor model, remaining 112 ICPs for the geometric accuracy assessment.

A high number of ground points was needed in this work because the reliability of RMSE value depends on the number of ICPs used to compute it. The National Standard for Spatial Data Accuracy (NSSDA) by the Federal Geographic Data Committee [35] recommends the use of a minimum of 20 ICPs. Nevertheless this size seems to be very small and some authors [36] and [37] suggest larger samples.

6 Results and Discussion

6.1 Sensor Orientation Errors

Table 2 shows the RMSE obtained in the nine GCPs at *X* and *Y* axes respectively. It can be seen that the sensor models that are demanding a higher number of GCPs to be computed (i.e., RPC2 and CCRS) are presenting a lower RMSE at GCPs than those who need fewer GCPs (i.e., RPC0 and RPC1). Really, RMSE at GCPs only shows a good accuracy estimation when the number of GCPs used is very high (i.e., the sensor models are computed with the highest redundancy).

When an assessment about geometric accuracy is required, the study has to be carried out over a high number of ICPs. In table 3, *X*, *Y* and planimetric RMSEs are showed. The sensor models CCRS and RPC2, for this order, show the worse results, with mean values of planimetric RMSE ($RMSE_p$) of 0.46 m and 0.41 m respectively. According to bibliography, CCRS model should present a great robustness over the full image using only a few GCPs [33], nevertheless, it is difficult to develop a parametric sensor model which reflects the physical reality of the complete viewing geometry for a sensor with an absence of detailed sensor information, such as GeoEye-1. For the RPC0 and RPC1, the $RMSE_p$ values were 0.34 m and 0.36 m respectively.

If the first results at the orientation phase obtained in this work are compared with those from IKONOS published by Aguilar et al. [8] a lot of similarities can be drawn. $RMSE_p$ for IKONOS were 0.60 m, 0.63 m and 1.09 m using RPC0, RPC1 and CCRS respectively. If these IKONOS results are normalized attending to the acquired nominal GSD (0.84 m for the IKONOS image used), the resulting $RMSE_p$ would be of 0.71 pixels for RPC0, 0.75 pixels for RPC1 and 1.30 pixels for CCRS. On the other hand, for GeoEye-1 with 0.46 m of acquired nominal GSD, the normalized $RMSE_p$ would be of 0.74 pixels, 0.78 pixels and 1.00 pixels for RPC0, RPC1 and CCRS respectively.

With only a bias-compensation adjustment of the supplied RPCs (i.e., RPC0 model), geopositioning accuracy at 55 ICPs of 0.1 m (0.2 pixels) in planimetry and 0.25 m (0.5 pixels) in height were reported by Fraser and Ravanbakhsh ([24] with a stereo-pair of GeoEye-1 and a single GCP. This level of metric performance will surpasses both the design expectations of the system and those inferred from experience with IKONOS. However, these wonderful results have not been generated from our single image.

GCPs	ICPs	Model	$RMSE_x$ (m)	$RMSE_y$ (m)
9	112	RPC0	0.22	0.24
	112	RPC1	0.22	0.21
	112	RPC2	0.09	0.20
	112	CCRS	0.02	0.14

Tab. 2 RMSE at X and Y axes obtained from GCPs during the sensor orientation of the GeoEye-1 satellite image.

GCPs	ICPs	Model	$RMSE_x$ (m)	$RMSE_y$ (m)	$RMSE_p$ (m)
9	112	RPC0	0.22	0.26	0.34
	112	RPC1	0.26	0.25	0.36
	112	RPC2	0.33	0.25	0.41
	112	CCRS	0.31	0.34	0.46

Tab. 3 RMSE at X and Y, and planimetric RMSE ($RMSE_p$) obtained from ICPs during the sensor orientation of the GeoEye-1 satellite image.

6.2 Orthorectification Errors

An assessment of the geometric accuracy was done for the orthoimage generated by RPC0 sensor model with 9 GCPs. 43 ICPs located on the ground were used to compute the final $RMSE_p$ in the orthoimage. The final panchromatic orthoimage had a planimetric accuracy of around 0.87 m. Although it can seem a very raised value (almost 1.9 times the acquires nominal GSD), you must bearing in mind the high off-nadir angle for our image (20.59º) and the relatively low accuracy of the DEM used ($RMSE_z$ of 1.34 m in the study area).

Using a similar DEM, planimetric accuracies of 1.04 m and 1.15 m were attained form orthoimages generated from QuickBird basic and IKONOS Geo Ortho Kit imagery [8].

6.3 Comparison from 1956 to 2010

The recent process of concentration of economic activities and population undergone by this coastal region has produced serious landscape and environmental alterations. The present work shows the changes happened in a section of the Almería coast included between Garrucha and Villaricos harbours during the last half century, concretely from 1956 to 2010.

In the beaches of Almería, the erosion processes have been very strong. Thus, between 1957 and 1996, more than 2.8 millions square meters of these beaches have been lost [38]. The main reasons for that erosive tendency, especially in the beach of Quitapellejos, are promoted by sediment reduction as results of an increasing urbanization of the littoral areas that provokes impervious zones that do not contribute sediments to the sea and the excessive extractions of sand from beach for the soil preparation in culture greenhouse.

Fig. 4 Orthoimage from American flight (year 1956) at nowadays as named Puerto Rey private state.

Fig. 5 Orthoimage from GeoEye-1 (year 2010) at nowadays named as Puerto Rey private state.

The construction of a dam at Cuevas del Almanzora and the canalization of the Almanzora river are events that have also diminished the contribution of sediments proceeding from this river. In this sense, Fig. 4 and 5 are showing the amazing proliferation of urbanizations in our study area during the last 50 years at the area nowadays occupied for the private state named as Puerto Rey.

On the other hand, shorelines, defined as the interface between sea and land, tend to retreat, with over 70% of the world's beaches experiencing coastal erosion. This presents a serious hazard to many coastal regions, where it is estimated that about 25% of productivity occurs and 60% of the population lives. Climate change, particularly accelerated sea-level rise, is expected to exacerbate this problem meaning that sensible management strategies are increasingly required to deal with the risks arising from coastal erosion. In addition to present day monitoring campaigns, coastal management relies on information about historic shoreline location and movement, and on predictions of future change.

With regards to our study area, Fig. 6 and 7 show the evolution of the shoreline at Quitapellejos beach from 1956 to 2010. Although numerous and expensive performances have been fulfilled during the last 15 years, such as breakwaters or regenerations of sands, these actions have not managed to stop the high rates of erosion in this zone.

Fig. 6 Shorelines of 1956 (yellow) and 2010 (red) over orthoimage from American flight (year 1956) at Quitapellejos beach.

Fig. 7 Shorelines of 1956 (yellow) and 2010 (red) over orthoimage from GeoEye-1 (year 2010) at Quitapellejos beach.

6.4 Further works

The growth in agriculture, increased urbanization and natural processes all contribute to the changing nature of land use and land cover around the globe. Remote sensing has been identified as a critical tool in understanding changes on a large and small scale, and currently several satellites are being employed to monitor and study the globe.

The high spatial resolution of GeoEye-1 (Fig. 8) or WorldView-2 enables the discrimination of fine details, like vehicles, shallow reefs and even individual trees in an orchard, and the high spectral resolution (especially in the case of WorldView-2) provides detailed information on such diverse areas as the quality of the road surfaces, the depth of the ocean, and the health of plants.

Four-band pan-sharpened, half-meter resolution imagery from GeoEye-1 have already used for accurately mapping red and grey canopy cover (to within 1.7 percent of field estimates), which are indicators of the severity of a current outbreak of mountain pine beetles in a lodge pole pine-dominated forest [23].

In our Research Projects the four-band of GeoEye-1 (Fig. 8), included in multispectral imagery with a spatial resolution of 2 m and fused imagery with a spatial resolution of 0.5 m, are going to be used to impervious zones classification in the study area, using object-oriented classification methods for mapping urban features .

These types of satellite imagery are going to be used for mapping beds of *Posidonia oceanica* in the Mediterranean Sea, where it is a dominant species forming monospecific beds in a structurally simple environment. As with other seagrass species, they play an important role in many coastal processes, contributing to sediment deposition, attenuating currents and wave energy and stabilizing unconsolidated sediments. The widespread loss of this species is attributed to excessive antropic pressure and other large-scale environmental changes. Some research works related to this focus have already been published using other satellite imagery such as SPOT 5 [39] and IKONOS [40]. Fig. 9 shows Near Infrared response of the seagrass at shallow waters in an area detailed in Fig. 8.

Fig. 8 Multispectral Orthoimage from GeoEye-1 (Nir,G,R).

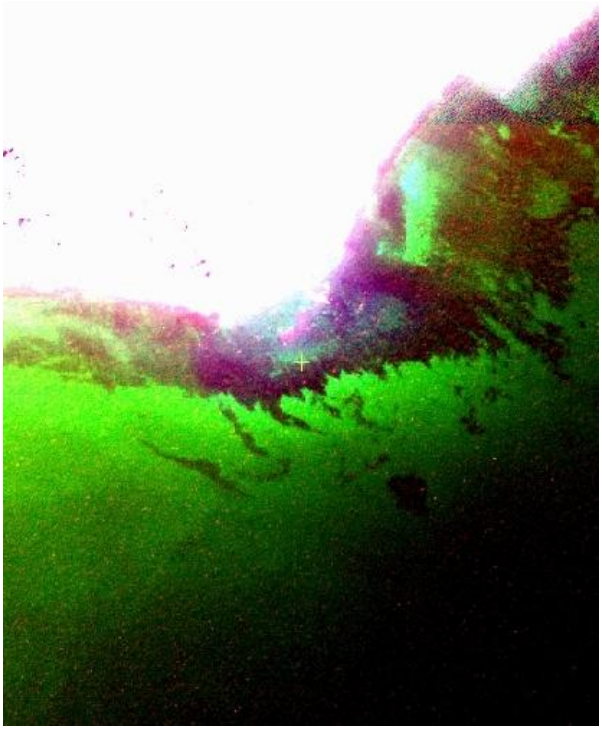

Fig. 9 Multispectral Orthoimage from GeoEye-1 (Nir,G,R) showing underwater coast detail.

One step further, with 8 tightly focused spectral sensors ranging from visible to near infrared, combined with 1.8 meter spatial resolution, WorldView-2 brings a high degree of detail to classification process, enabling a finer level of discrimination and improving decision-making. Coastlines, shoals and reefs are some of the most dynamic and constantly changing regions of the

globe. Monitoring and measuring these changes is critical to marine navigation and an important tool in understanding our environment. For our coastal project, near shore bathymetry has a great importance. It is currently being calculated using high-resolution multispectral satellite imagery. However, with the introduction of WorldView-2's higher resolution, increased agility and Coastal Blue band (400-450 nm), bathymetric measurements could be substantially improve both in depth and accuracy [25].

7 Conclusions

The best results in the sensor orientation phase for GeoEye-1 Geo panchromatic image were obtained when RPC0 model was used although followed very closely by RPC1. The RMSEp for sensor orientation phase was of 0.34 m. RPC2 and CCRS models showed the worst geometric accuracies.

With regards to the orthorectified images from GeoEye-1, the planimetric RMSE at final orthoimage presented a value of 0.87 m. In any case, the sensor model RPC0 generated the best results. Because of it, when we have the vendor's RPC file, RPC0 should be the method used in the process of orthorectification of GeoEye-1 Geo imagery.

The new possibilities of the last generation of Very High Resolution satellites due to both geometrical and spectral resolution for feature classification, bathymetric measurements, vegetative analysis or change detection are still for exploring.

Acknowledgement

This work was supported by the Spanish Ministry for Science and Innovation (Spanish Government) and the European Union (FEDER founds) under Grant Reference CTM2010-16573, corresponding to the Research Project named "Generacion de datos georreferenciados de muy alta resolucion a partir de imagenes de los satélites GeoEye-1 y WorldView-2". The authors also appreciate the support form Andalusia Regional Government, Spain, through the Excellence Research Project RNM-3575.

References

[1] J. Croft, 2008. *Prodigious Mapping Capabilities, Spatial resolution and Geo-location ability, GeoEye's next-generation Imaging Satellite*. GeoInformatics, 4 (2008) pp 18-23.

[2] C.S Fraser, 2002. *Prospect for mapping from high-resolution satellite imagery*. The 23rd Asian Conference on Remote Sensing (2002), Kathmandu, Nepal, unpaginated CD ROM.

[3] S. Kay, P. Spruyt, K. Alexandrou, 2003. *Geometric quality assessment of orthorectified VHR space image data*. Photogrammetric Engineering and Remote Sensing, 69(5) pp 484-491.

[4] J. Chmiel, S. Kay, P. Spruyt, 2004. *Orthorectification and geometric quality assessment of very high spatial resolution satellite imagery for Common Agricultural Policy purposes*. Proceeding of the XXth International Archives of the Photogrammetry.

[5] J. Pecci, F. Cano, G. Maza, 2004. *Generación de una ortoimagen QuickBird del año 2003 de la Comunidad Autónoma de la Región de Murcia: metodología y resultados*. XI Congreso Métodos Cuantitativos, Sistemas de Información Geográfica y Teledetección, Murcia, Spain, pp 301-312.

[6] F.J. Aguilar, F. Carvajal, M.A. Aguilar, F. Agüera, 2007. *Developing digital cartography in rural planning applications*. Computers and Electronics in Agriculture, 55(2) pp 89-106.

[7] M.A. Aguilar,F.J. Aguilar, F. Carvajal, F. Agüera, L. Estrada, 2006. *Geometric accuracy of Ikonos Geo Panchromatic Orthoimage Products*. Revue française de photogrammétrie et de télédétection, 184 pp 5-10.

[8] M.A. Aguilar, F. Agüera, F.J. Aguilar, F. Carvajal, 2008. *Geometric accuracy assessment of the orthorectification process from very high resolution satellite imagery for Common Agricultural Policy purposes*. International Journal of Remote Sensing, 29(24) pp 7181-7197.

[9] C.S. Fraser, E. Baltsavias, A. Gruen, 2002a. *Processing of Ikonos imagery for submetre 3D positioning and building extration*. ISPRS Journal of Photogrammetry and Remote Sensing, 56 pp 177-194

[10] C. Weber and T. Ranchin, 2003. *Extraction of urban features in Strasbourg, France: Comparison of two fusion algorithms for Quickbird MS and Pan data*. 2nd GRSS/ISPRS Joint Workshop on "Data Fusion and Remote Sensing over Urban Areas".

[11] S.D. Lee, J. Shan, J. Bethel, 2003. *Class-guided buildings extraction from Ikonos imagery*. Photogrammetric Engineering and Remote Sensing, 69(2) pp 143-150.

[12] V. Mesev, 2005. *Identification and characterisation of urban bulding patterns using IKONOS imagery and point-based postal data.* Computers, Environment and Urban Systems, (29): 541-557.

[13] T. Kim, T.Y. Lee, K.O. Kim, 2006. *Semiautomatic building line extraction from Ikonos images through monoscopic line analysis*. Photogrammetric Engineering and Remote Sensing, 72 pp 541-549.

[14] S.D. Mayunga, D.J. Coleman, Y. Zang, 2007. *A semi-automated approach for extracting buildings from QuickBird imagery applied to informal settlement mapping*. International Journal of Remote Sensing, 28(10) pp 2343-2357.

[15] P. Gamba, F. Dell'Acqua, G. Lisini, G. Trianni, 2007. *Improved VHR urban area mapping exploting object boundaries*. IEEE Transactions on Geoscience and Remote Sensing, 45(8) pp 2676-2682.

[16] D. Yan and Z. Zhao, 2003. *Road Detection from Quickbird Fused Image Using HIS Transform and Morphology*. 2nd GRSS/ISPRS Joint Workshop on "Data Fusion and Remote Sensing over Urban Areas".

[17] X. Jin, C.H. Davis, 2005. *An integrated system for automatic road mapping from high-resolution multi-spectral satellite imagery by information fusion*. Information Fusion, 6 pp 257-273.

[18] J. Nichol, and C.M. Lee, 2005. *Urban vegetation monitoring in Hong Kong using high resolution multispectral images*. International Journal of Remote, 26(5) pp 903-918.

[19] J.A. Martínez-Casasnovas, M. Concepción Ramos, D. Vallés, 2009. *Análisis de la relación entre las propiedades del suelo, el índice de vigor del cultivo y el rendimiento en un viñedo de la D.O. Costers del Segre (Lleida)*. XIII Congreso de la Asociación Española de Teledetección, Calatayud.

[20] F. Agüera, M.A. Aguilar, F.J. Aguilar, 2006. *Detecting greenhouses changes from QuickBird*

imagery on the Mediterranean coast. Internacional Journal of Remote Sensing, 27(21) pp 4751-4767.

[21] F. Agüera, F.J. Aguilar, M.A. Aguilar, 2008. *Using texture analysis to improve per-pixel classification of very high resolution images*. ISPRS Journal of Photogrammetry and Remote Sensing, 63(6) pp 635-646.

[22] D.H.A. Al-Khudhairy, I. Caravaggi, S. Giada, 2005. *Structural Damage Assessments from Ikonos Data Using Change Detection, Object-Oriented Segmentation, and Classification Techniques*. Photogrammetric Engineering and Remote Sensing, 71(7) pp 825-837.

[23] P.E. Dennison, A.R. Brunelle, V.A. Carter, 2010. *Assessing canopy mortality during a mountain pine beetle outbreak using GeoEye-1 high spatial resolution satellite data*. Remote Sensing of Environment 114 (2010) pp 2431-2435.

[24] C.S Fraser and M. Ravanbakhsh, 2009. *Georeferencing Accuracy of GeoEye-1 Imagery*. Photogrammetric Engineering and Remote Sensing, 75(6) pp 634-638.

[25] DigitalGlobe, 2009. *The Benefits of the 8 Spectral Bands of WorldView-2*. Website: http://worldview2.digitalglobe.com/docs/WorldView-2_8-Band_Applications_Whitepaper.pdf. Accessed 3 Feb 2011.

[26] Andalusian Government, 2005. *Modelo Digital del Terreno de Andalucía. Relieve y orografía*. Junta de Andalucía, Sevilla, Spain (On DVD).

[27] F.J. Aguilar, I. Fernández, M.A. Aguilar, J.L. Pérez, J. Delgado, J.G. Negreiros, 2010. *Shaded-reliefs matching as an efficient technique for 3d georeferencing of historical digital elevation models*. International Archives of Photogrammetry, Remote Sensing and Spatial Information Science, Volume XXXVIII, Part 8.

[28] C.V. Tao and Y. Hu, 2001. A *comprehesive study of the rational function model for photogrammetric processing*. Photogrammetric Engineering and Remote Sensing, 67(12) pp 1347-1357.

[29] C.S. Fraser and T. Yamakewa, 2004. *Insights into affine model for high-resolution satellite sensor orientation*. ISPRS Journal of Photogrammetry and Remote Sensing, 58(2004) pp 275-288.

[30] T. Toutin, 2004. *Review article: Geometric processing of remote sensing images: models, algorithms and methods.* International Journal of Remote Sensing, 25(10) pp 1893-1924.

[31] Y. Hu and C.V. Tao, A. Croitoru, 2004. *Understanding the rational function model: methods and applications*. Proceeding of the XXth International Archives of the Photogrammetry, Remote Sensing and Spatial Information Sciences, 35(Part B5), Istambul, Turkey, unpaginated CD ROM.

[32] J. Grodecki and G. Dial, 2003. *Block adjustment of high-resolution satellite images described by rational polynomials*. Photogrammetric Engineering and Remote Sensing, 69(1) pp 59-68.

[33] P. Cheng, T. Toutin, Y. Zhang, M. Wood, 2003. *QuickBird- Geometric correction, path and block processing and data fusion*. Earth Observation Magazine, 12(3) pp 24-30

[34] T. Toutin, 2003. *Error tracking in Ikonos geometric processing using a 3D parametric model*. Photogrammetric Engineering and Remote Sensing, 69(1) pp 43-51.

[35] FGDC, 1998. *Geospatial Positioning Accuracy Standards Part 3: National Standard for Spatial Data Accuracy*. Website: http://www.fgdc.gov/standards/projects/FGDC-standards-projects/accuracy/part3/chapter3, U.S. Federal Geographic Data Committee, Reston, Virginia. Accessed: 2 Feb 2011).

[36] Z. Li, 1991. *Effects of check points on the reliability of DTM accuracy estimates obtained from experimental tests*. Photogrammetric Engineering & Remote Sensing, 57(10) pp1333–1340.

[37] M.A. Aguilar, F.J. Aguilar, F. Agüera, 2008. *Assessing geometric reliability of corrected images from very high resolution satellites*. Photogrammetric Engineering and Remote Sensing, 74(12) pp 1551-1560.

[38] A. Viciana, 2001. *Erosión costera en Almería, 1957-1995*. Ed. Instituto de Estudios Almerienses. Diputación de Almería.

[39] V. Pasqualini, C. Pergent-Martini, G. Pergent, M. Agreil, G. Skoufas, L. Sourbes, A. Tsirika, 2005. *Use of SPOT 5 for mapping seagrasses: An application to Posidonia oceanic*. Remote Sensing of Environment, 94 (2005) pp 39-45.

[40] A. Fornes, G. Basterretxea, A. Orfila, A. Jordi, A. Alvarez, J. Tintore, 2006. *Mapping Posidonia oceanica from IKONOS*. ISPRS Journal of Photogrammetry & Remote Sensing, 60 (2006) pp 315-322.